ROYAL SOCIETY OF CHEMISTRY

PAPER

CrossMark
click for updates

One-step bimodel grafting *via* a multicomponent reaction toward antifouling and antibacterial TFC RO membranes†

Ying Pan,[a] Liujia Ma,[a] Song Lin,[b] Yufeng Zhang,[a] Bowen Cheng[a] and Jianqiang Meng*[a]

Simple methods for dual functional modification of membrane surfaces have been rarely reported but are highly desirable for the fabrication of antifouling and antibacterial membranes. In this work, we exploit a multicomponent reaction, Ugi-4CR (Ugi four-component reaction), to prepare novel antifouling and antibacterial reverse osmosis (RO) membranes. With the aid of the high number of residual carboxyl groups on a commercial polyamide RO membrane as the anchor and methyl isocyanoacetate as a component, a hydrophilic macromolecular component, methoxy poly(ethylene glycol) aldehyde (MPEG-CHO), and an amino-terminated antibacterial component, tris(2-aminoethyl)amine (TAEA) or sulfamethoxazole (SMZ), were grafted onto the surface in a single step *via* the Ugi-4CR. The surfaces of the original and modified membranes were characterized by ATR-FTIR, XPS, TG, WCA, FESEM and AFM measurements. The antifouling performance was evaluated by cross-flow filtration of protein and inorganic salt solution. The antibacterial performance was assessed by the shake flask method. The results show that the Ugi-4CR was successfully conducted on the RO membrane surface and that MPEG-CHO and the antibacterial agents were successfully grafted. The surface roughness decreased and surface the hydrophilicity improved upon modification. After 48 h fouling experiments, the obtained PA-*g*-PEG/TAEA and PA-*g*-PEG/SMZ membranes showed obviously lower flux attenuation ratios and higher flux recovery ratios than the original membrane in both cases when fouled by protein or inorganic salt. In addition, the bacterial concentrations in the suspensions shook with the modified membranes were much lower than that of the original membrane. As for the PA-*g*-PEG/SMZ membrane, hardly any bacterial growth was seen, even after 24 h culture. In contrast to current multi-step grafting processes, this work reports a "one pot" procedure with two functional groups grafted simultaneously under very mild conditions without the use of any catalyst.

Introduction

With world-wide industrialization and the increasing population, in recent years, serious water scarcity and urgent demand for fresh water resources have emerged. As a consequence, there is a great need for the exploration of new water sources and waste water reclamation. Among various solutions,[1] reverse osmosis desalination has been considered to be the most effective method to relieve water scarcity.[2] RO has occupied 70% of the seawater desalination market and has already been widely used in wastewater reuse, seawater and brackish water desalination, pure water fabrication, *etc.*[3]

[a] *State Key Laboratory of Separation Membranes and Membrane Processes, Tianjin Polytechnic University, Tianjin 300387, China. E-mail: jianqiang.meng@hotmail.com; jianqiang_meng@126.com; Fax: +86 22 83955055; Tel: +86 22 83955386*

[b] *Institute of Medical Equipment, Academy of Military Medical Science, Tianjin 300161, China*

Aromatic polyamide (PA) thin-film composite (TFC) RO membrane has dominated the commercial RO membrane market for 30 years since the breakthrough discovery made by Cadotte and his co-workers in 1985.[4] It has a multi-layer structure, mainly consisting of three layers: a non-woven fabric layer (~110 μm) at the bottom, a micro-porous polysulfone support layer (40 to 70 μm) in the middle and an ultra-thin functional polyamide layer (100 to 300 nm) on the top, which is normally prepared by interfacial polymerization of *m*-phenylenediamine (MPD) in the aqueous phase and trimesoyl chloride (TMC) in the organic phase on the polysulfone support layer. Compared with other RO membranes, this TFC membrane exhibits high water permeability, high salt rejection, high resistance to pressure compaction, wide operation temperature and pH ranges, and high stability to biological attack.[5]

RO has been regarded as a mainstream desalination technology for its excellent separation performance; however, it severely suffers from membrane fouling, which involves organic, inorganic and microbial pollution. Membrane fouling is the main obstacle restricting the further development and

This journal is © The Royal Society of Chemistry 2016

J. Mater. Chem. A, 2016, **4**, 15945–15960 | 15945

increases the cost of RO operations. Pollutants in water tend to be adsorbed and attached to the membrane surface due to hydrophobic interactions and electrostatic attraction, leading to a fouling layer on the membrane surface. Meanwhile, the bacteria multiply rapidly, producing large amounts of metabolic secretions which may accelerate the formation of the fouling layer. All these unfavorable factors will lead to a decline in water flux and permeate quality, eventually necessitating rinsing of the membrane, with degradation of performance as a result.[6] Therefore, it is of great significance to improve the antifouling and antibacterial performance of RO membranes to prolong their service life.

It is well known that RO membranes are prone to fouling because of the interaction between the membrane surface and pollutants, which is strongly related to the surface hydrophilicity, charge and roughness of the membrane. For organic and inorganic pollution, membranes modified with a smooth and hydrophilic surface with a similar charge to that of the pollutants seem to present good antifouling properties.[7,8] By contrast, biofouling is a greater problem and is the major cause of RO membrane fouling.[9,10] Because of the extremely high reproduction rate of the bacteria, it is uncontrollable and impossible to completely eliminate biofouling by simple pretreatment. In this context, it is essential to introduce effective antimicrobial agents onto the membrane surface to inhibit reproduction.[11] Surface grafting and organic/inorganic hybrid modification are the optimal and common solutions considered for biofouling suppression.[10,12]

Numerous surface modification methods have been reported to address membrane fouling problems. Surface grafting of hydrophilic groups and antibacterial agents can efficiently alleviate organic fouling and biofouling, respectively.[13–15] However, the composition of waste water in real cases is extremely complicated and can foul the membrane *via* multiple mechanisms. Current modification methods feature immobilization of a single functional group in one step; this has the limitation of only addressing one particular type of pollution. Most efforts to achieve antifouling RO membranes only address a single type of fouling behavior.[16,17] In the case of dealing with the complicated fouling mechanisms involved in practical applications, multiple-step reactions must be conducted to endow membranes with both antifouling and antibacterial properties. For example, Zhao *et al.* first blended poly((ethylene glycol) methacrylate-*co*-methylacrylic acid) (PEGMA-MAA) nanogel with PES to provide the membrane with good resistance to protein adhesion. Then, *in situ* silver nanoparticle immobilization was conducted to endow the membrane with remarkable inhibition and killing capabilities toward both *S. aureus* and *E. coli* bacteria.[18] Gao *et al.* used a multi-step procedure combining surface-initiated atom transfer radical polymerization (ATRP) and a quaternization reaction to fabricate antifouling and antibacterial PVDF membranes. First, hydrophilic poly(2-hydroxyethyl methacrylate) (PHEMA) brushes were grafted onto the surface of a poly(vinylidene fluoride) (PVDF) membrane *via* ATRP. Then, antibacterial poly(2-(dimethylamino)ethyl methacrylate) (PDMAEMA) was covalently bound with HEMA to endow the membrane with

antibacterial properties. To further improve the antibacterial properties, the modified membrane was then treated with alkyl bromide *via* a quaternization reaction.[19] Isao Sawada *et al.* grafted acrylamide onto a PES hollow fiber membrane *via* photo-grafting for organic fouling alleviation. Then, *in situ* silver nanoparticle formation in the grafted layer was conducted to confer antibacterial properties by immersing the grafted membrane into a silver nitrate solution.[20] To simply the modification process, simple and efficient grafting chemistries are required for one-step surface modifications to fabricate multifunctional membranes.

Multicomponent reactions (MCRs) have emerged as useful methods because the combination of several components to generate new products in a single step is extremely economical and efficient.[21,22] In recent years, multicomponent reactions based on carboxylic acids have been used for the synthesis of functional polymers.[23,24] The Ugi four-component reaction (Ugi-4CR) is a typical multicomponent reaction (MCR) involving a wide range of monomers with biocompatible side-groups.[25,26] Ugi-4CR involves the coupling of four chemical functionalities, including carboxylic acids, amino groups, aldehydes, and isocyanides, to prepare diversely substituted amides with finely tunable structures under very mild reaction conditions without the use of catalyst in a "one-pot procedure".[27,28] Ugi-4CR has recently been introduced as a novel, efficient and useful material synthesis and modification tool in many areas, such as chemical biology and pharmaceutical technology.[29,30] Very recently, the Ugi-4CR reaction was used for surface modification. The Ugi reaction, RAFT polymerization and π–π stacking were conducted in one pot to modify pristine CNTs to improve their solubility in both aqueous and organic solvents.[31]

Fortunately, commercial RO membranes usually contain high numbers of carboxylic group residues on their surfaces; we envisage that the RO membrane can be regarded as a source of carboxylic acid groups, facilitating the occurrence of Ugi-4CR. Methoxy poly(ethylene glycol) aldehyde (MPEG-CHO) was chosen as the aldehyde component due to the very high hydrophilicity of PEG, thus endowing the membrane with good resistance to organic and inorganic fouling.[32,33] An amino-terminated antibacterial agent, tris(2-aminoethyl)amine (TAEA) or sulfamethoxazole (SMZ), was used as the amino component to restrain the growth and adhesion of the bacteria in the feed.[34] Finally, methyl isocyanoacetate was selected as the isocyanide compound because of its low cost and ready availability. It serves as the connection to tether the above two functional components onto the membrane surface. The one-step bimodel grafting strategy is elucidated in Fig. 1.

The purpose of this work is to develop a simple and versatile strategy for surface modification by means of Ugi-4CR for improving the antifouling and antibacterial properties of RO membranes. The chemical structure of the membrane surface was characterized by ATR-FTIR and XPS. The surface morphology was observed by FESEM and AFM. The hydrophilicity was analyzed by water contact angle (WCA) measurements. The antifouling performance was evaluated by cross-flow filtration of bovine serum protein (BSA) and hard inorganic salt
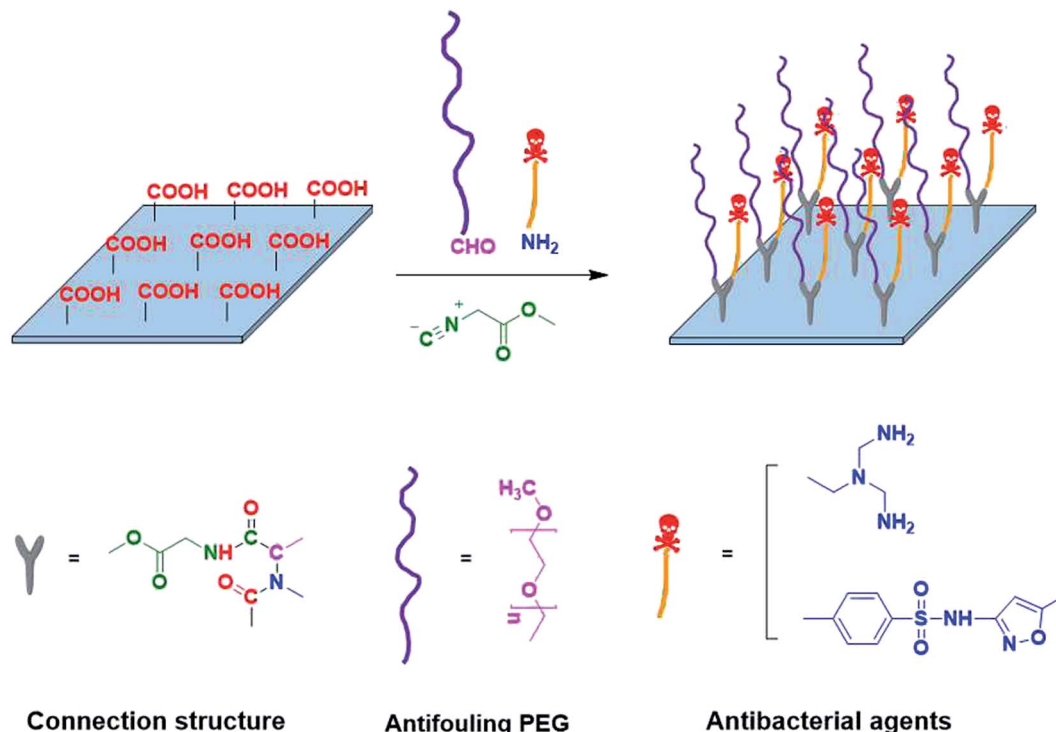
15946 | *J. Mater. Chem. A*, 2016, **4**, 15945–15960

This journal is © The Royal Society of Chemistry 2016

Fig. 1 One-step bimodel grafting *via* a multicomponent reaction to fabricate antifouling and antibacterial TFC RO membranes.

solution. The antibacterial properties were assessed quantitatively using the shake flask method.[35]

Experimental

1. Materials

The commercial TFC RO membrane used in this study was LCLE membrane, purchased from DOW Chemical Co. Ltd. (Minneapolis, MN, USA). LCLE membrane is a low-energy TFC RO membrane product composed of a polysulfone support membrane and an aromatic polyamide layer which is fabricated by the interfacial polymerization of an aromatic amine and an acyl chloride. Methoxy poly(ethylene glycol) aldehyde (MPEG-CHO) was purchased from Jenkem Technology Co. Ltd. (Beijing, China). Tris(2-aminoethyl)amine (TAEA), sulfamethoxazole (SMZ) and methyl isocyanoacetate were purchased from J&K Chemical Co. (China). Bovine serum albumin (BSA) was purchased from Sigma-Aldrich. Methanol, sodium chloride (NaCl), calcium chloride (CaCl$_2$), magnesium sulfate (MgSO$_4$), sodium bicarbonate (NaHCO$_3$) and sodium nitrate (NaNO$_3$) were purchased from Kermel Chemical Reagent Co. Ltd. (Tianjin, China). *Escherichia coli* (DH5α, Gram-negative) and *Staphylococcus aureus* (ATCC 6538, Gram-positive) were purchased from Bio Rc Co. Ltd. (Shanghai, China). Phosphate buffered saline solution (PBS, 0.03 mol L^{-1}) (2.84 g of Na$_2$HPO$_4$, 1.36 g of KH$_2$PO$_4$, 1 L of DI water) was prepared in house prior to use. All chemicals were analytical grade and were used as received. De-ionized (DI) water was obtained from a Millipore MilliQ system (18.2 M Ω^{-1} cm at 25 °C, 1.2 ppb TOC, pH = 6.9, Billerica, MA, USA). The membrane samples were rinsed with DI water for 4 h to remove the membrane additives and surface impurities, then dried in air before analysis.

2. Surface modification of LCLE membrane

LCLE membrane was modified by conducting the Ugi-4CR on the surface of the RO membrane. In a typical procedure, using TAEA as the antibacterial agent, the RO membrane samples (20 cm × 4 cm) were immersed in 100 mL of a methanol solution of MPEG-CHO (10 mmol L^{-1}), methyl isocyanoacetate (10 mmol L^{-1}) and TAEA (10 mmol L^{-1}). To facilitate the reaction, MPEG-CHO and TAEA were mixed and stirred for 20 min prior to the addition of the other two reactants. The whole mixture was stirred under nitrogen atmosphere for 12 h at 25 °C. The obtained modified membranes were rinsed thoroughly with DI water and dried in a vacuum oven at 25 °C for 24 h before measurements. The modification procedure using SMZ as the antibacterial agent was the same as that described above. The two modified membranes were designated as PA-*g*-PEG/TAEA and PA-*g*-PEG/SMZ, respectively.

3. Membrane surface characterization

The chemical structure of the membrane surface was investigated by ATR-FTIR spectra using a Vector 22 FTIR spectrometer (Bruker, Germany). The membrane samples were entirely rinsed with DI water and then dried at 25 °C in a vacuum oven before analysis. ATR-FTIR spectra were recorded in the wave number range of 600 to 4000 cm^{-1}.

X-ray photoelectron spectroscopy (XPS) was used to analyze the surface chemical composition of the membranes. This was

performed using a ThermoFisher K-alpha X-ray photoelectron spectrometer (Thermo Scientific, USA) with a monochromatic Al-Kα X-ray source ($h\nu$ = 1486.6 eV) at a pass energy of 93.9 eV. XPS spectra were obtained by sweeping the electron binding energy over 0 to 1000 eV with a resolution of 1 eV, followed by a high resolution scan of the C 1s region.

The grafting on the membrane surface was also analyzed by thermo-gravimetric analysis (TG). After delaminating the polyester non-woven fabric support from the backside, the membrane was immersed in chloroform to dissolve polysulfone. Then, the polyamide (PA) layer was removed from the solution and dried at 40 °C in a vacuum oven for 24 h. After that, TG analysis was conducted under continuous heating conditions from room temperature (25 °C) to 800 °C. The heating rate was kept constant at 10 °C min^{-1} in a nitrogen atmosphere.[36]

The morphologies of the membrane surface and cross-section were observed by field emission scanning electron microscopy (FESEM, Hitachi S-4800, Japan) under high vacuum conditions. Imaging was conducted at 3 kV with a working distance of 7.7 mm. The dry membrane samples were mounted on aluminum stubs and coated with Au before imaging. For the cross-section image sampling, the non-woven fabric layer was delaminated before quenching in liquid nitrogen. Atomic force microscopy (AFM, CSPM5500, Being Nano-Instruments, China) equipped with a scanning probe was also performed to quantitatively analyze the surface roughness of RO membranes. The tapping mode was chosen using a tip fabricated from silicon (125 μm in length with 300 kHz resonance frequency). An area of 10 μm × 10 μm was scanned at a speed of 10 lines per second.

The water contact angle (WCA) of the membrane surface was measured by a drop shape analysis system (DSA100, Krüss, Switzerland) using the circle–fitting method at 25 °C and 60% relative humidity. Droplets of DI water (2 μL) were placed at different spots of the membrane surface. The obtained value was an average of three measurements.

The surface charge of the membranes was determined by measuring the zeta potentials as a function of feed pH using the streaming potential method. The measurements were performed in a background solution containing 0.1 mmol L^{-1} KCl. The temperature was maintained at 25 °C and the pH was adjusted in the range of 3 to 10. The samples were pretreated with 0.1 mmol L^{-1} KCl solution overnight before testing. The zeta potential value was calculated from the streaming potential according to the Fairbrother and Mastin equation.[37]

4. Membrane permeation measurements

The RO performance was measured using a laboratory-made cross-flow-type apparatus at 1.5 MPa using 2000 ppm NaCl solution as the feed at 25 °C and a pH of 7.0.[38] The effective membrane area of the test cell was 18.75 cm^2. The permeation flux (J) and salt rejection (R) were measured at least three times for every sample and were calculated from the following equations:

$$J = \frac{V}{A \times t} \tag{1}$$

where V is the penetration liquid volume (L), A is the effective surface area of the membrane (m^2) and t is the penetration time (h).

$$R = \left(1 - \frac{C_p}{C_f}\right) \times 100\% \tag{2}$$

where C_p and C_f are the salt concentrations of the penetrate and the feed (μs cm^{-1}), respectively, which were measured by a conductance meter (EL30, METTLER TOLEDO, Switzerland).

5. Evaluation of antifouling properties

Organic fouling experiments. Protein is an important membrane foulant known to cause very rapid surface accumulation and permeability loss. Many researchers have used BSA as a typical material for organic pollution simulation.[39] A 2000 ppm NaCl solution containing 200 ppm BSA was used as the feed solution. The antifouling performance was evaluated by cross-flow filtration at 25 °C, 1.5 MPa. The pH of the feed solution was adjusted to be around 4.7, the isoelectric point of BSA. Under these conditions, BSA has the poorest solubility and the strongest hydrophobic interaction, thus promoting the fouling process. All membranes were pressurized beforehand with 2000 ppm NaCl for 2 h to obtain a stable water flux (J_0). Then, the feed solution was switched to NaCl/BSA solution. The fouling resistance was evaluated by recording the permeate flux (J_t) as a function of testing time and compared with the initial value (J_0) to analyze the flux decline ratio. After 48 h of fouling, all membrane samples were rinsed with DI water for 2 h; then, the feed was changed back to 2000 ppm NaCl solution and the membrane flux was remeasured as J_c to calculate the flux recovery ratio.

The antifouling properties were evaluated with several parameters, including total flux decline ratio DR$_t$, flux recovery ratio FRR, reversible flux decline ratio DR$_r$ and irreversible flux decline ratio DR$_{ir}$.[40] The equations are as follows:

$$DR_t = \left(1 - \frac{J_t}{J_0}\right) \times 100\% \tag{3}$$

where J_t is the water flux at time t (L m^{-2} h^{-1}) and J_0 is the initial flux (L m^{-2} h^{-1}).

$$FRR = \frac{J_c}{J_0} \times 100\% \tag{4}$$

where J_c is the water flux after cleaning (L m^{-2} h^{-1}).

$$DR_r = FRR - \frac{J_t}{J_0} \times 100\% \tag{5}$$

$$DR_{ir} = DR_t - DR_r \tag{6}$$

Obviously, DR$_t$ is the sum of DR$_r$ and DR$_{ir}$; FRR is the characteristic index. A higher value of FRR and a lower value of DR$_t$ indicate better antifouling properties for a particular membrane.

Inorganic fouling experiments. The inorganic fouling resistance of the membranes was evaluated by cross-flow filtration of a solution containing a mixture of inorganic salts, simulating

15948 | J. Mater. Chem. A, 2016, 4, 15945–15960

This journal is © The Royal Society of Chemistry 2016

the composition of groundwater, with high hardness. The feed solution was prepared by dissolving 0.580 g of CaCl₂, 0.476 g of MgSO₄, 4.085 g of NaHCO₃ and 0.998 g of NaNO₃ in 10 L of DI water. The main ions and their corresponding concentrations are shown in Table 1. The solution pH was adjusted to 8.5 with 0.1 mol L^{-1} NaOH. The concrete operation process was similar to the BSA testing procedure. The initial flux value was measured with pure water instead of 2000 ppm NaCl solution.

6. Evaluation of antibacterial properties

The antibacterial properties of the membrane were assessed by the shake flask method using *E. coli* as the model Gram-negative bacteria and *S. aureus* as the model Gram-positive bacteria.[41] The bacteria were cultivated in nutrient broth (15 g L^{-1} tryptone, 5 g L^{-1} phytone, 5 g L^{-1} sodium chloride, pH = 7.0) and placed in an incubator-shaker for 24 h at 37 °C. Then, the bacteria suspension was diluted to 4×10^5 CFU mL^{-1} (colony-forming units per milliliter) with 0.03 mol L^{-1} PBS solution. The bacterial concentration was determined based on the absorbance at 660 nm. Under these conditions, the diluted bacteria suspension still contained a certain amount of nutrient broth, which can provide the bacteria with favorable living circumstances. Then, 0.75 g of membrane samples were cut into pieces of 5 mm × 5 mm and transferred into a wide mouth bottle containing 70 mL of PBS solution and 5 mL of diluted bacteria suspension. A bacteria suspension in PBS without added membrane samples was used as the blank control. The wide mouth bottles were sealed and shaken at 25 °C for 24 h. 100 μL of bacterial suspension was pipetted out every hour and diluted 100 times with PBS solution, then was subsequently coated on a nutritive agar plate (15 g of agar dissolved in 1 L of nutrient broth) carefully. The plates were sealed and incubated at 37 °C for 24 h. Finally, the bacteria colonies present on the plate were counted to calculate the bacterial concentration of every wide mouth bottle and the bacterial inhibition rate of every sample by formula (7) and (8).

$$N = Z \times R \tag{7}$$

where N represents the bacterial concentration in the wide mouth bottles (CFU mL^{-1}), Z is the average value of bacteria colonies presented on every agar plate (CFU) and R is the dilution ratio.

$$K = \left(1 - \frac{N_m}{N_o}\right) \times 100\% \tag{8}$$

where K is the bacterial inhibition rate of the membrane sample (%), N_m is the bacterial concentration corresponding to each membrane sample (CFU mL^{-1}) and N_o is the bacterial concentration corresponding to the blank control (CFU mL^{-1}).

All the samples must be sterilized in UV for at least 1 h before operation. All the supplies mentioned above were autoclaved for 20 min at 121 °C with a high pressure steam sterilization pot. The whole procedure was conducted in an ultra clean bench without contact with the atmosphere. Each extraction and coating operation was conducted twice in case of error.

Results and discussion

1. Ugi-4CR

Membrane surface grafting has been the subject of intensive research for several decades. However, most surface grafting methods are still confined to building monolayers with single functionalities. Grafting methods allowing for construction of hierarchical grafting layers with multiple functionalities, such as block copolymers and polymers with nonlinear topologies, are still rare.

To address the membrane fouling issue, which is driven by a complex mechanism, it is ideal to tether the corresponding chemical agents in a simple way. Multicomponent reactions should be considered for their feature of simultaneously attaching several functionalities in a single step. Furthermore, the segment sequence determined by the reaction mechanism ensures homogeneous distribution of the different functionalities. Finally, Ugi-4CR is also attractive for its mild conditions; neither catalyst nor heating is required during the process, which is advantageous compared with other multi-component reactions.

According to the mechanism of Ugi-4CR shown in Fig. 2, the added amine, aldehyde and isocyanate are equivalent, and the preferential reaction of the amino and aldehyde groups will facilitate the whole procedure. We dissolved MPEG-CHO and TAEA (or SMZ) in methanol and stirred the mixture for 20 to 30 min until the solution became clear; then, RO membrane and methyl isocyanoacetate were added. The reaction time and reagent concentrations were optimized to provide a good balance between the permeation properties and antifouling performance. We found that a high reactant concentration led to better antifouling performance but lower membrane flux. Finally, the reaction conditions of 10 mmol L^{-1} for each component and 12 h reaction time were selected to prepare the grafted membranes.

It should be noted that more than one amine group in a TAEA molecule can participate in the reaction, forming a cyclic structure with double tethered PEG chains, although the possibility is low due to the steric hindrance of the bulky PEG chains. It is believed that this side reaction can hardly affect the obtained membrane performance due to the presence of numerous amine groups.

2. ATR-FTIR spectra

ATR-FTIR spectra of the original and modified membrane surfaces are shown in Fig. 3. For the two modified membranes,
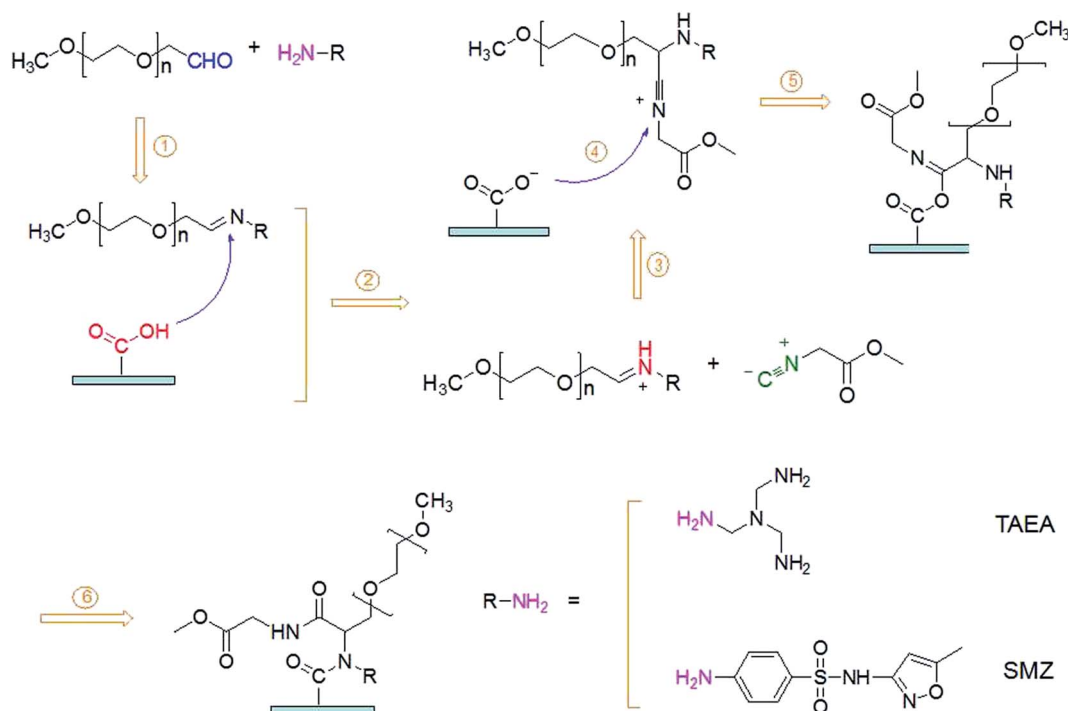
Table 1 The composition of the feed solution for the inorganic fouling experiments

Ion	Ion concentration (mg L^{-1})
Ca^{2+}	208.9
Mg^{2+}	9.5
Na$^+$	925.2
HCO$_3^-$	296.6
SO$_4^{2-}$	380.8
Cl^{1-}	1584.6

This journal is © The Royal Society of Chemistry 2016

J. Mater. Chem. A, 2016, **4**, 15945–15960 | **15949**

Fig. 2 The proposed mechanism of the Ugi-4CR on the RO membrane.

the absorption band at 2878 cm^{-1} is markedly enhanced after modification due to the grafting of PEG, which contains many CH$_2$ groups. The bands at 1669, 1609, and 1540 cm^{-1} correspond to C=O stretching (amide I), hydrogen bonded C=O stretching (amide I), and N–H in-plane bending (amide II), respectively. These bands are characteristic of the polyamide structure in the active layer.[42] Interestingly, we observed that these adsorptions intensified after surface grafting. This phenomenon is ascribed to amide group formation in the Ugi-4CR. For the PA-g-PEG/SMZ membrane, two new absorption bands emerged at 1037 cm^{-1} and 1344 cm^{-1}; these are attributed to the stretching of S=O and N–O in the oxazole rings of

Fig. 3 ATR-FTIR spectra of the original (a), PA-g-PEG/TAEA (b) and PA-g-PEG/SMZ (c) membranes.

the SMZ molecules. All these results indicate the success of the Ugi-4CR on the surface of the PA RO membrane.

3. XPS measurements

XPS measurements were conducted to further analyze the changes in the chemical composition of the membrane surface upon modification. The wide spectra and C 1s core-level spectra are shown in Fig. 4. For the original membrane, there are three major emissions in the wide spectra at 284.6 eV, 400.0 eV and 532.0 eV which are attributed to the binding energies of C 1s, N 1s, and O 1s, respectively. The C 1s core-level spectrum of the original membrane can be legibly curve-fitted with three symmetric peaks with binding energies at 284.6 eV, assigned to C–H/C–C species, at 286.0 eV, assigned to C–O/C–N species, and at 288.0 eV, assigned to C–C=O species.[43] The PA-g-PEG/TAEA membrane actually has a very similar curve profile to the spectrum of the original membrane. In spite of that, the intensity of the C–C/C–H bonds appears to be greater than that of the original membrane. This is due to the grafting of PEG, which contains large amounts of CH$_2$–CH$_2$. As for the PA-g-PEG/SMZ membrane, two new emissions emerge in the wide spectra at 167.29 eV and 227.72 eV, attributed to the binding energies of S 2p and S 2s, respectively; these originate from the elemental sulfur in SMZ. Additionally, the corresponding C–S adsorption peak appears at 285.0 eV in the fitted C 1s core-level spectra.

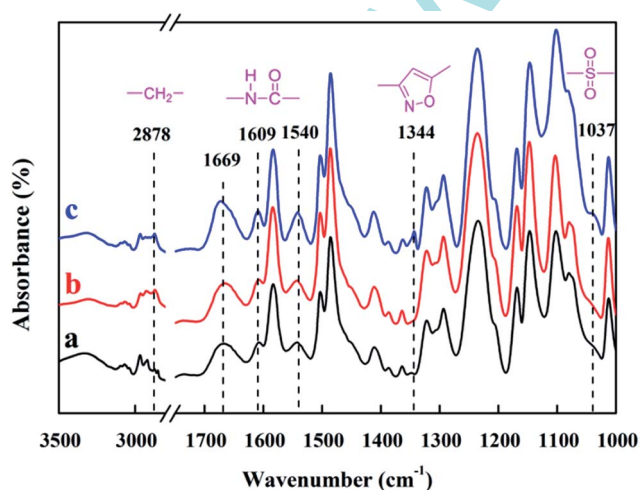## 4. TG analysis

The ATR-FTIR and XPS results strongly suggest that PEG and antibacterial agents were successfully grafted to the surface of the RO membrane. The thermogravimetric analysis (TG) shown
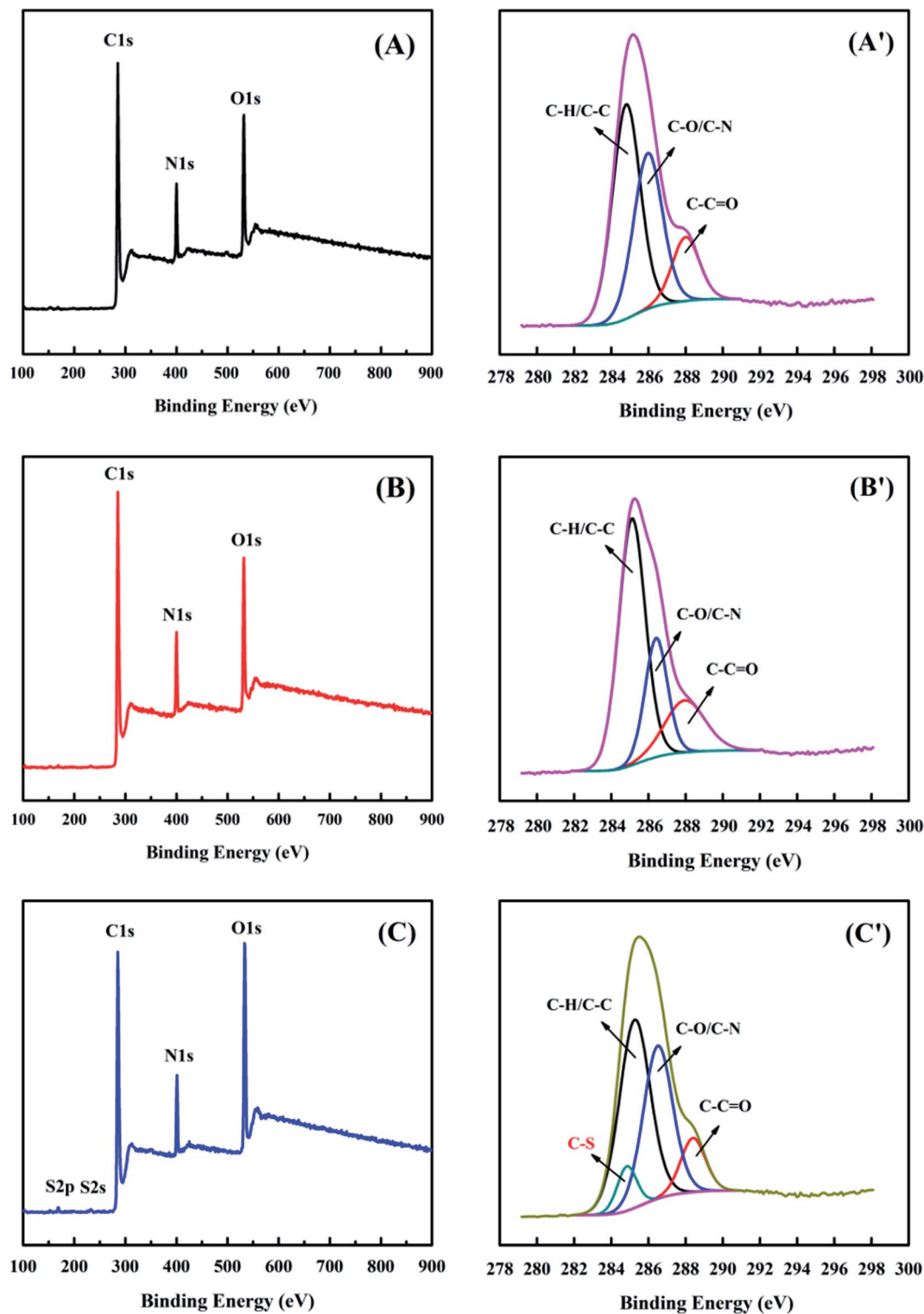
15950 | J. Mater. Chem. A, 2016, **4**, 15945–15960

This journal is © The Royal Society of Chemistry 2016

Fig. 4 XPS wide scan spectra (A–C) and C 1s core-level spectra (A′–C′) of the original (A and A′), PA-*g*-PEG/TAEA (B and B′) and PA-*g*-PEG/SMZ (C and C′) membranes.

in Fig. 5 further verifies the occurrence of Ugi-4CR. Compared with the original membrane, the two modified membranes show new degradation at 400 °C, indicating that a completely new product has been generated on the membrane surface, which is attributed to Ugi-4CR.

5. Membrane surface morphology

The changes in the morphologies of the membrane surfaces upon modification were observed by FESEM and AFM. The images are shown in Fig. 6 and 7. The original thin-film
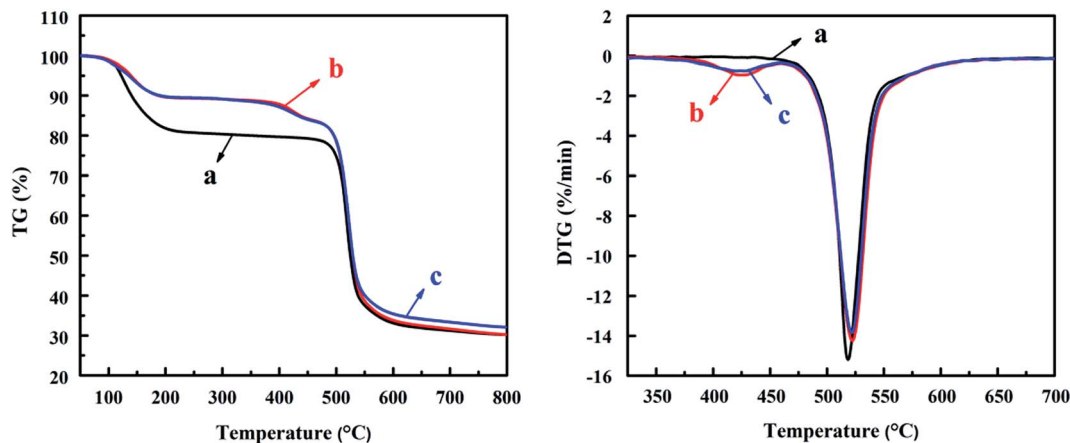
This journal is © The Royal Society of Chemistry 2016

J. Mater. Chem. A, 2016, **4**, 15945–15960 | **15951**

Fig. 5 TG analysis of the original (a), PA-*g*-PEG/TAEA (b) and PA-*g*-PEG/SMZ (c) membranes.

composite PA membrane has a typical "ridge-and-valley" structure. The surface is characterized by high roughness. However, the modified membranes are somewhat different. Although the typical "ridge-and-valley" structure still exists, it appears that the introduction of PEG and amino hydrophilic groups filled the valley areas, leading to smoother membrane surfaces. We also attempted to measure the thicknesses of the PA layers by SEM measurements of membrane cross-sections. However, it is difficult to differentiate the PA layer from the polysulfone support layer, even at 5000× magnification (see ESI Fig. S1†).

In order to verify the SEM observations, the roughness of the membrane surfaces was quantitatively analyzed by AFM; the results are shown in Fig. 7. The root mean square roughness (Rms) values of the original, PA-*g*-PEG/TAEA and PA-*g*-PEG/SMZ membranes are 83.9 nm, 61.9 nm and 65.2 nm, respectively, indicating that the modification process significantly decreases the surface roughness.

6. WCA measurements

It is well known that the hydrophilicity of the membrane surface is one of the most important factors influencing membrane performance, especially its antifouling properties.[44] Fig. 8 shows the WCA values measured by the circle–fitting method. After 30 s of wetting, the contact angle decreased from 69.7° for the original membrane to 40.7° (PA-*g*-PEG/TAEA) and 41.5° (PA-*g*-PEG/SMZ) upon modification, indicating that the modified membranes show much better wettabilities than the original membrane. Since the modified membranes have lower surface roughness than the original membrane, we believe the lower WCA values for the modified membranes can be ascribed to the successful introduction of hydrophilic PEG chains.

7. Zeta potential analysis

The surface charge properties of the RO membranes before and after modification were measured by the streaming potential method over the pH range of 4.0 to 10.0. The results are shown
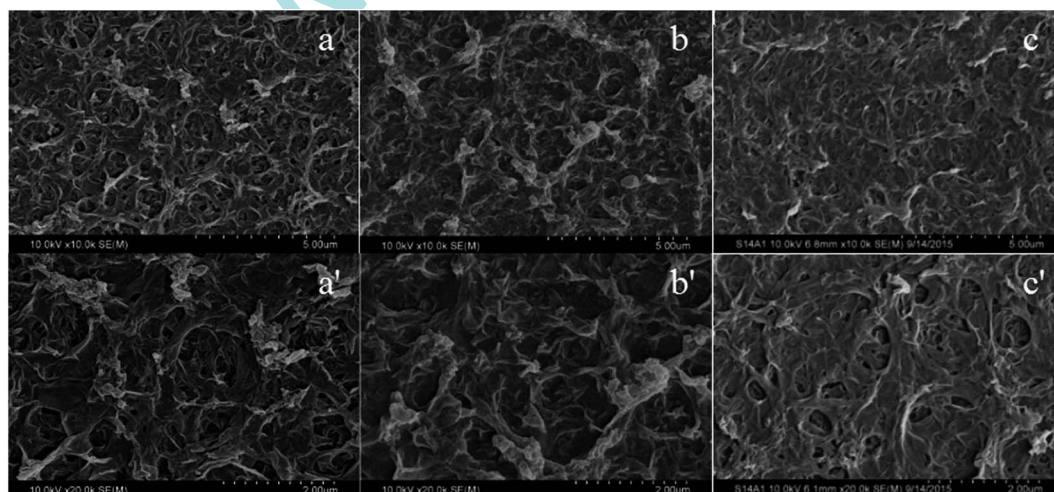

Fig. 6 FESEM images of the original (a and a'), PA-*g*-PEG/TAEA (b and b') and PA-*g*-PEG/SMZ (c and c') membranes (a–c 10 000×, a'–c' 20 000×).

15952 | *J. Mater. Chem. A*, 2016, **4**, 15945–15960
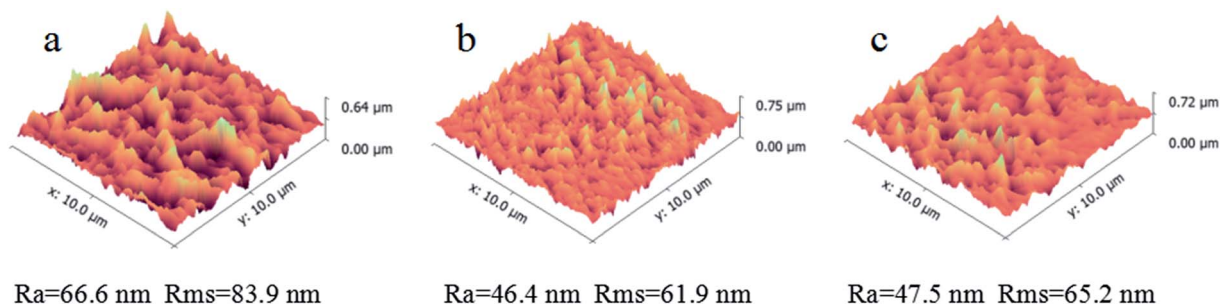
This journal is © The Royal Society of Chemistry 2016

Fig. 7 AFM images of the original (a), PA-*g*-PEG/TAEA (b) and PA-*g*-PEG/SMZ (c) membranes.
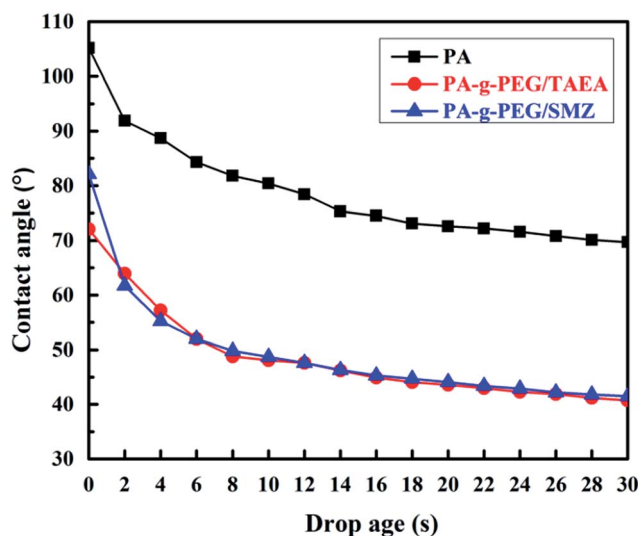
Fig. 8 The water contact angles of the original, PA-*g*-PEG/TAEA and PA-*g*-PEG/SMZ membranes.

demonstrated by the SEM and AFM results, also leads to lowered surface roughness and a decreased active filtration area; the membrane flux decreases as a result.[45] The modification process has no essential effect on the salt rejection of the
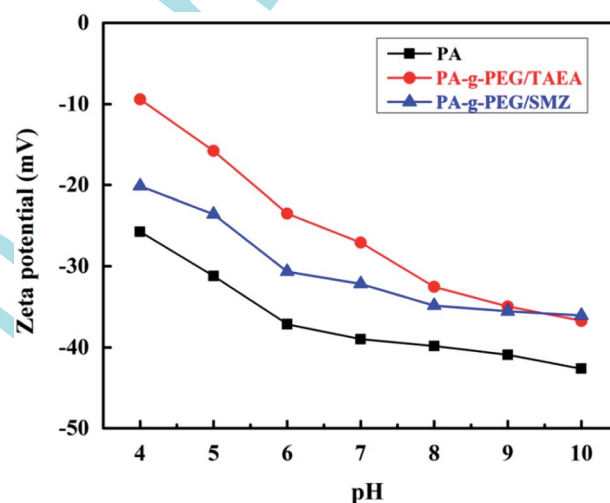

Fig. 9 Zeta potentials of the original, PA-*g*-PEG/TAEA and PA-*g*-PEG/SMZ membranes.

in Fig. 9. The original membrane features a typical negatively charged surface, ascribed to the high number of residual carboxyl groups. The surfaces of the two modified membranes show slightly weakened negative charges upon Ugi-4CR due to the consumption of carboxyl groups. This phenomenon is more obvious for the PA-*g*-PEG/TAEA membrane due to the grafting of positively charged amino groups.

8. Membrane permeation properties

Fig. 10 shows the alternation of the permeation flux and salt rejection of the membranes upon modification. It is apparent that the fluxes of the modified membranes dramatically decrease after surface grafting from the original flux of 64.0 L m^{-2} h^{-1} to 40.8 L m^{-2} h^{-1} for the PA-*g*-PEG/TAEA membrane and 38.9 L m^{-2} h^{-1} for the PA-*g*-PEG/SMZ membrane. This phenomenon is believed to be due to the increased membrane permeation resistance caused by the grafted layer. Although the grafted macromolecules have excellent hydrophilicity, which is beneficial to the sorption of water molecules in the membrane, the influence of the hindered diffusion is far greater than the advantage from the promoted sorption. In addition, the filling of the valley area by the grafted polymer, which has been
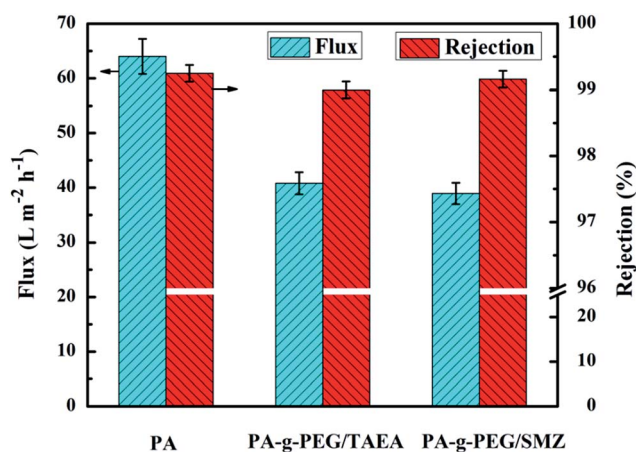

Fig. 10 Water flux and salt rejection of the original, PA-*g*-PEG/TAEA and PA-*g*-PEG/SMZ membranes (testing conditions: 2000 ppm NaCl aqueous solution, 1.5 MPa, 25 °C and pH of 7.0).

This journal is © The Royal Society of Chemistry 2016

J. Mater. Chem. A, 2016, 4, 15945–15960 | 15953

membrane, which remains above 99.0% for both the original and modified membranes. Therefore, we can draw the conclusion that the modification process does not jeopardize the innocent PA structure or alter its bulk transport properties.

9. Antifouling performance

Organic fouling. The membrane antifouling performance was evaluated by cross-flow filtration of model foulants in a laboratory scale testing bench. BSA was used as the model foulant to simulate organic fouling. Fig. 11 shows the evaluation of membrane flux (a) and rejection (b) with permeation time. Before adding BSA, the initial water flux values of the original, PA-*g*-PEG/TAEA and PA-*g*-PEG/SMZ membranes were 64.0 L m^{-2} h^{-1}, 40.8 L m^{-2} h^{-1} and 38.9 L m^{-2} h^{-1}, respectively. After changing the feed to BSA solution, the permeation flux decreased for all the membrane samples. The curves of all the membranes show a two-stage profile: a rapid flux drop at the beginning, which is more profound for the original membrane, followed by a stage where the membranes show gradual flux attenuation.[46] We believe that the membrane–BSA interaction predominates in the first stage, where rapid adsorption and deposition of BSA onto the membrane surface causes

a remarkable flux decline. In the second stage, the BSA–BSA interaction may predominate.[47] The BSA adsorption onto and desorption from the membrane approaches equilibrium; therefore, the membrane flux becomes steady for the modified membranes. On the other hand, the flux decline for the original membrane was still rapid, indicating that the deposition of BSA onto the membrane surface was much quicker than its desorption. It should be noted that the solution pH was adjusted to 4.7, the isoelectric point of BSA, which was supposed to provoke the most severe hydrophobic–hydrophobic interactions between BSA molecules or between BSA and the membrane surface. The accumulation of BSA was exacerbated. As a result, the dehydration and denaturation of BSA would inevitably form a dense cake layer. In the whole testing process, the original membrane suffered from a dramatic flux decline, and the decline ratio was much higher than that of the modified membranes. After 48 h of fouling, the flux of the original membrane was only 62.7% of the initial value, while the PA-*g*-PEG/TAEA and PA-*g*-PEG/SMZ membranes both remained above 90.0%, indicating obviously improved antifouling performance. This phenomenon is attributed to the increased surface hydrophilicity and reduced roughness due to the grafting of
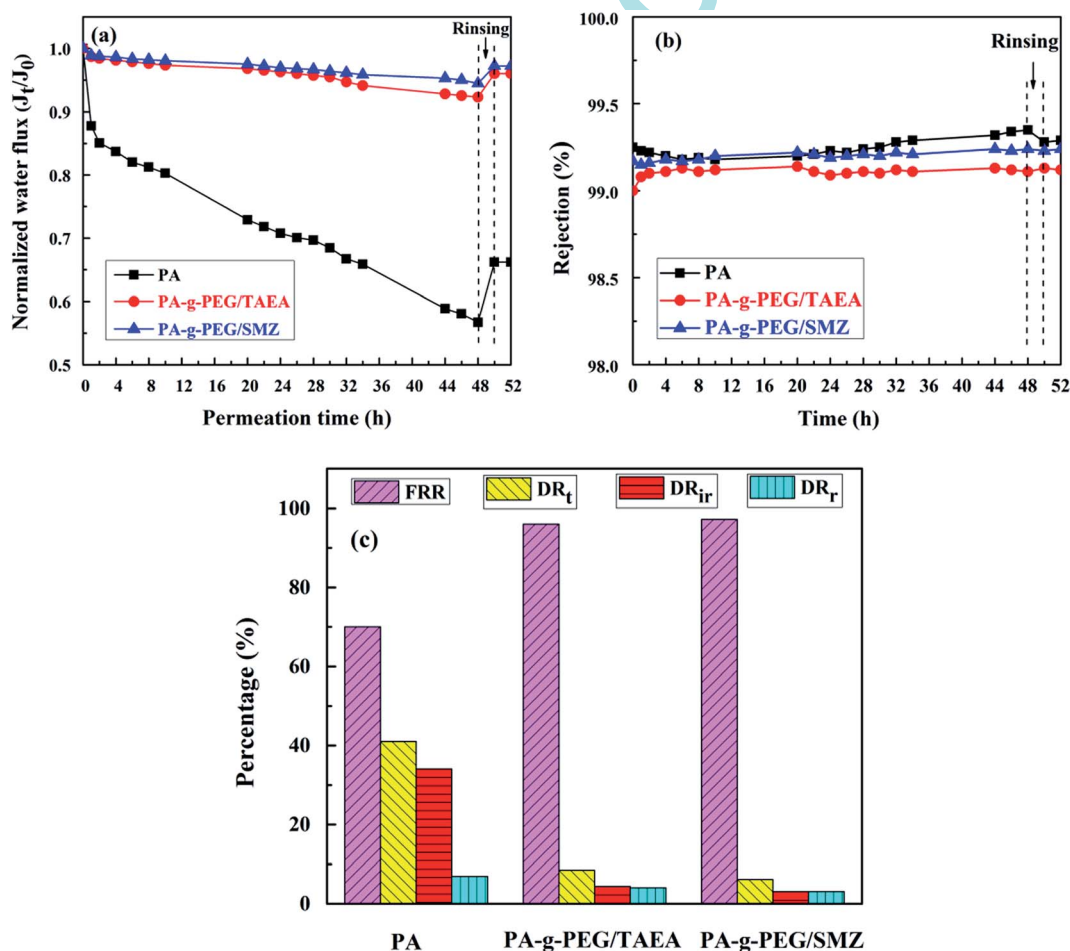

Fig. 11 (a) Normalized water flux, (b) salt rejection and (c) flux decline ratios and flux recovery ratios of the original, PA-*g*-PEG/TAEA and PA-*g*-PEG/SMZ membranes tested with BSA (testing conditions: 2000 ppm NaCl + 200 ppm BSA feed solution, 1.5 MPa, 25 °C and pH of 4.7).

PEG molecules.[48] Firstly, PEG is capable of bonding with a number of water molecules through hydrogen bonding, constructing a stable hydration layer on the membrane surface around PEG, which acts as an effective barrier for BSA attachment.[49] Secondly, the considerable C–O bonds endow the PEG chain with good flexibility so that it can stretch freely, forming a prominent steric hindrance effect to resist pollution attack.[50]

We can see from Fig. 11(b) that the change of salt rejection with fouling time is not notable. The salt rejection of all the samples remained slightly over 99.0% during the fouling process. However, a gradual increase in the rejection of the original membrane was observable in the fouling process, while the rejections of the two modified membranes were basically stable. This result should be due to the cake layer accumulated by BSA, leading to minimization of the convective transport of salt ions. We can also see a drop in the rejection for the original membrane after rinsing, which is due to the rinsing out of some BSA foulants. As for the modified membranes, because of the stable existence of the grafted layer, the salt rejection remained almost permanent during the whole process, even when the samples were rinsed with pure water.

Fig. 11(c) presents the quantitative analysis of the flux recovery ratios and the flux decline ratios. After testing with BSA for 48 h, all the samples were rinsed with pure water for 2 h. The flux recovery ratios (FRR) of the two modified membranes are higher than that of the original membrane. Moreover, the total flux decline ratios (DR$_t$) of the modified membranes are obviously lower. We believe the minimized irreversible flux decline ratios (DR$_r$) of the modified membranes actually account for their decreased DR$_t$. BSA fouling is basically an irreversible pollution process for the original membrane. In comparison, half of the declined flux can be recovered for the modified membranes due to the superior antifouling properties of the modified membranes. The PA-g-PEG/SMZ membrane shows slightly better antifouling performance, which may be related to its more negatively charged membrane surface, leading to better protein repellent properties.

Inorganic fouling. The antifouling behavior against inorganic salts was evaluated by cross-flow filtration of a salt solution with high hardness, simulating groundwater composition. The normalized water flux and salt rejection values of the membrane samples are shown in Fig. 12(a) and (b). The curves
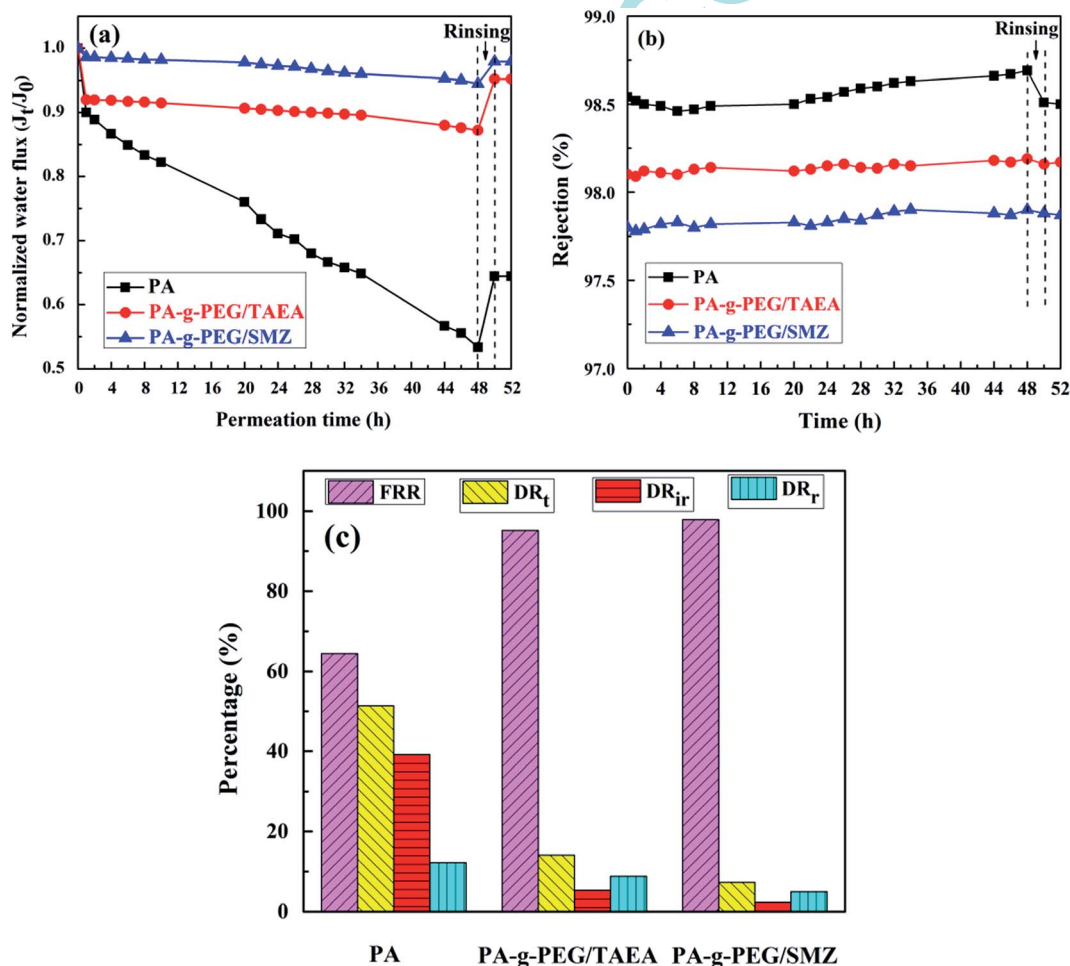

Fig. 12 (a) Normalized water flux, (b) salt rejection and (c) flux decline ratio and flux recovery ratio of the original, PA-g-PEG/TAEA and PA-g-PEG/SMZ membranes tested with a high salinity solution (testing conditions: the high salinity feed solution shown in Table 1, 1.5 MPa, 25 °C and pH 8.5).

This journal is © The Royal Society of Chemistry 2016

J. Mater. Chem. A, 2016, **4**, 15945–15960 | **15955**

show similar trends to those of BSA. The initial water permeation flux values of the original, PA-g-PEG/TAEA and PA-g-PEG/SMZ membranes were 76.8 L m^{-2} h^{-1}, 43.2 L m^{-2} h^{-1} and 41.6 L m^{-2} h^{-1}, respectively. At the early stage of the fouling process (about 2 h), the flux of all samples underwent significant attenuation, mainly caused by concentration polarization.[51] As shown in Fig. 12(a), the original membrane had a higher flux reduction rate than the two modified membranes after a 48 h fouling process. The flux lost nearly half of the initial value for the original membrane, while the two modified membranes only attenuated by around 10.0%. Similar to the tendency of the BSA fouling process, the salt rejection of the original membrane increased slightly at the end of the fouling process and dropped again after hydraulic cleaning. Meanwhile, the PA-g-PEG/TAEA and PA-g-PEG/SMZ membranes maintained their initial values for almost the whole process due to the stable grafted layer. The FRR and DR$_t$ were analyzed in detail and are shown in Fig. 12(c). Two modified membranes show lower flux decline ratios and higher recovery ratios, benefiting from the good hydrophilicity and flexibility of the PEG chains. The proportion of DR$_{ir}$ in DR$_t$ is not only dramatically lower than that of the original membrane, but is also much lower than the DR$_r$ proportion of the modified membranes. Similar conclusions can be drawn from the above results that irreversible fouling dominates the flux decline of the original membrane, and the declined flux can barely be recovered by rinsing; meanwhile, for the PA-g-PEG/

TAEA and PA-g-PEG/SMZ membranes, the reversible part is obviously higher, which is beneficial for long-term use.

Fig. 13 shows the FESEM images of the original, PA-g-PEG/TAEA and PA-g-PEG/SMZ membranes fouled by high salinity solution for 48 h and then rinsed with pure water for 2 h. Obviously, there are large salt precipitates on the original membrane surface, while the two modified surfaces are clean and no visible crystallization can be seen. The above results suggest that modification reduces the deposition of inorganic salts and improves the resistance of the membrane to inorganic fouling. This is due to the hydration and steric hindrance effects mentioned in the BSA test; also, more importantly, PEG is in fact an intrinsic scale inhibitor. The numerous C–O–C groups in PEG molecules can combine with metal ions such as Ca^{2+} and Mg^{2+} by complexation, thus preventing the metal ions from crystallizing with acid groups on the membrane surface, resulting in weakened concentration polarization.[52,53]

All the above results were obtained under equal transmembrane pressures. It can be argued that the original membrane should be fouled quicker because a higher mass permeates it during the fouling process due to its intrinsic high flux. To further verify the superiority of the fouling resistance of the modified membranes, we repeated the antifouling tests of BSA and inorganic salts in equal initial flux mode. The transmembrane pressure of the original membrane was adjusted to 0.9 MPa to achieve basically equal initial flux for all the RO
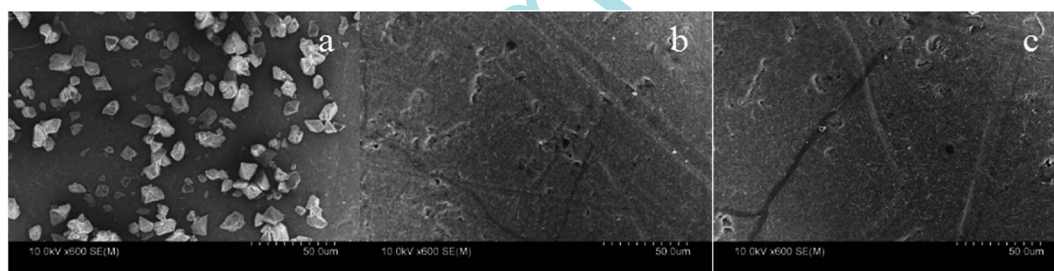

Fig. 13   FESEM images of original (a), PA-g-PEG/TAEA (b) and PA-g-PEG/SMZ (c) membranes fouled by inorganic salt after rinsing.
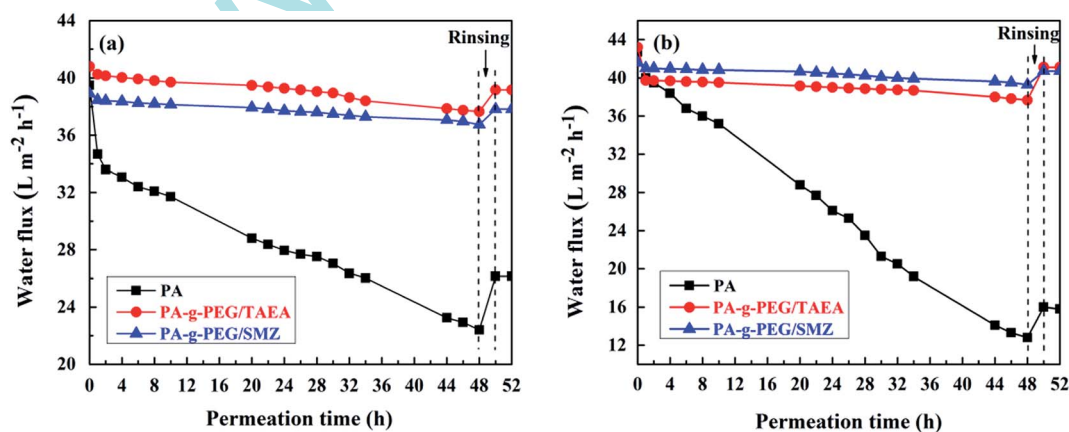

Fig. 14   The evolution of membrane flux with permeation time for membranes fouled by BSA (a) and inorganic salts (b) in equal initial water flux mode (testing conditions: (a) 2000 ppm NaCl + 200 ppm BSA feed solution, an initial flux of 40.0 L m^{-2} h^{-1} for the three membranes, 25 °C and pH 4.7; (b) the high salinity feed solution shown in Table 1, an initial flux of 42.0 L m^{-2} h^{-1} for the three membranes, 25 °C and pH 8.5).

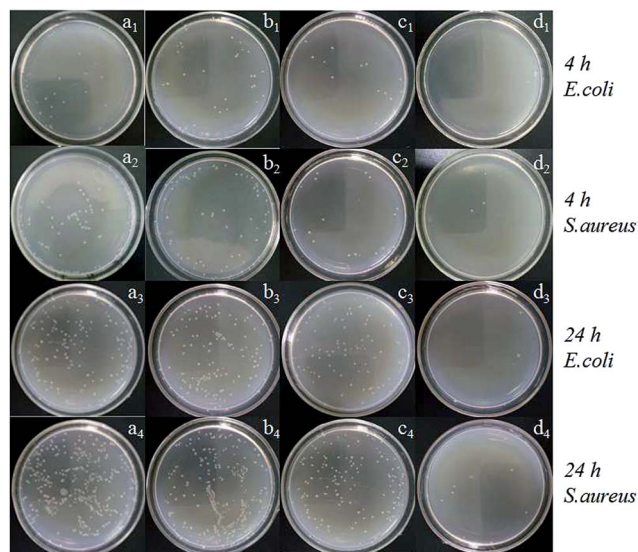**Fig. 15** Images of *E. coli* (a_1–d_1, a_3–d_3) and *S. aureus* (a_2–d_2, a_4–d_4) colonies on agar plates corresponding to the blank control (a_1–a_4) and the original (b_1–b_4), PA-*g*-PEG/TAEA (c_1–c_4) and PA-*g*-PEG/SMZ (d_1–d_4) membranes after 4 h (a_1–d_2) and 24 h (a_3–d_4) cultures.

fouling resistance between the original and modified membranes is more obvious, further confirming the superior fouling resistance of the modified membranes.

10. Antibacterial performance

The inhibition of membrane samples towards bacterial growth in suspension was monitored by the shake flask method. The bacterial concentration and bacterial inhibition rate related to every sample can be calculated by counting the bacteria colonies presented on an agar plate according to formulas (7) and (8). In this work, the antibacterial performance was assessed in detail for 4 h and 24 h bacteria cultures.

The images of *E. coli* and *S. aureus* colonies presented on agar plates corresponding to the blank control and the original, PA-*g*-PEG/TAEA and PA-*g*-PEG/SMZ membranes are shown in Fig. 15. The bacterial suspension was first shook for 4 h and incubated at 37 °C. As shown in the images, the number of colonies related to the original membrane was almost equivalent to that of the blank control; however, for the PA-*g*-PEG/TAEA and PA-*g*-PEG/SMZ membranes, the number of colonies significantly decreased. The original membrane has no obvious effect on the intrinsic growth of bacteria, while the two modified membranes show obvious inhibition performance; this is especially true for the PA-*g*-PEG/SMZ membrane.

TAEA and SMZ were characterized by broad spectrum antimicrobial properties at low bacterial density. To further explore their antibacterial activities at high bacterial concentrations,

membrane samples. The results are shown in Fig. 14. We can see that the variation trends are almost the same as those in equal trans-membrane pressure mode. Interestingly, the flux decline for the original membrane is in fact even more severe than that tested at 1.5 MPa. As a result, the difference in the
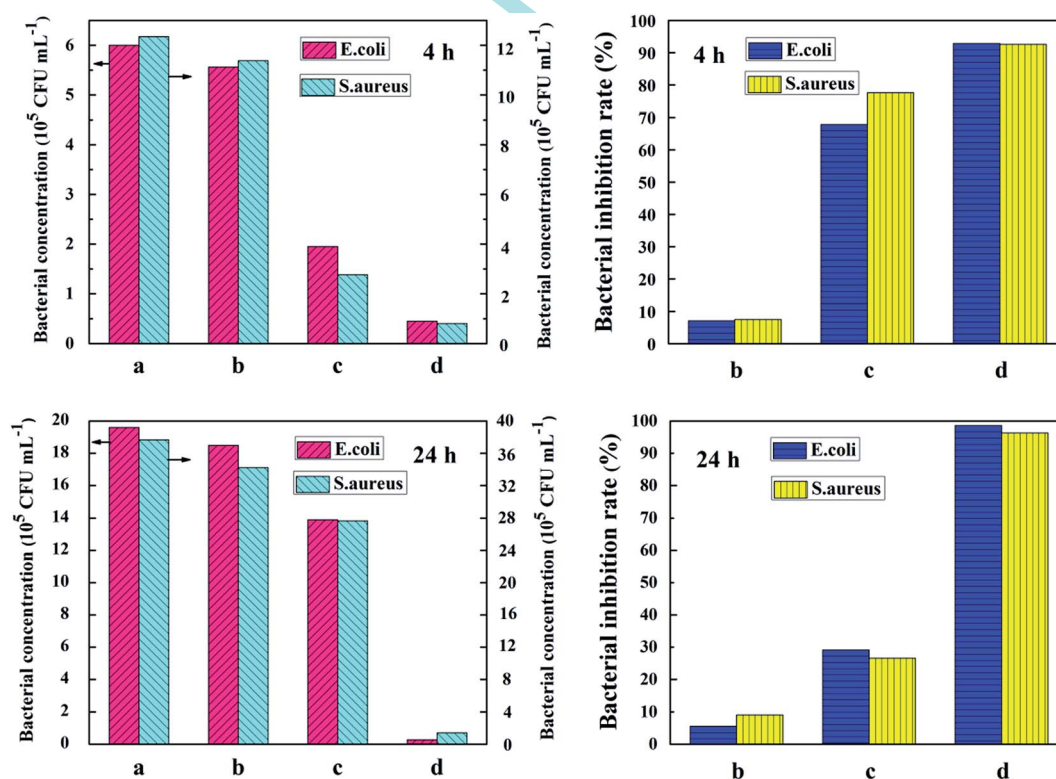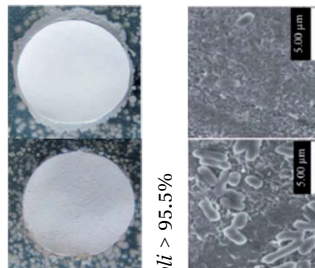

Fig. 16 The bacterial concentrations and bacterial inhibition rates corresponding to the blank control (a) and the original (b), PA-*g*-PEG/TAEA (c) and PA-*g*-PEG/SMZ (d) membranes tested for 4 h and 24 h.

This journal is © The Royal Society of Chemistry 2016

J. Mater. Chem. A, 2016, **4**, 15945–15960 | **15957**

Table 2 Comparison of antifouling and antibacterial properties of RO membranes

Starting membrane	Modification method	Antifouling properties				Antibacterial properties		Reference
		Test conditions	Flux (L m^{-2} h^{-1})	DR$_t$ (%)	FRR (%)	Test conditions	Efficiency	
LCLE	One-step bimodel grafting *via* Ugi-4CR	200 ppm BSA@1.5 MPa Inorganic salt@1.5 MPa	38.9 41.6	5.6 6.6	97.2 97.9	*E. coli* *S. aureus*	98.6% 96.3%	This work
Lab-made	(1) Preparation of MPD-terminated PEG (2) Interfacial polymerization	250 ppm BSA@1.4 MPa	38.0	21.0	92.0	*E. coli* *B. subtilis*	10 to 100 times greater antibacterial activity	57
LCLE	(1) Synthesis of random terpolymer P(MDBAC-r-am-r-HEMA) (2) Dip coating of RO membrane followed by cross-linking	100 ppm BSA@1.5 MPa	55.2	15.8	90.3	*E. coli*		38
SWC4+	(1) Synthesis of PEI-coated AgNPs (2) Synthesis of thiol terminated polymer (3) Synthesis of PAA-propargyl amide (4) LBL assembly (5) Grafting of polymer brushes	Non applicable				*E. coli* > 95.5%		12
TE	(1) Dip coating of an ultrathin metal-polyphenol layer on the membrane surface (2) Immobilization of PVP onto a metal-polyphenol precursor layer	200 ppm BSA@1.55 MPa 400 ppm lysozyme@1.55 MPa	70.2 69.4	46.6 31.6	79.7 73.4	Non applicable		58
SHN	(1) Dip coating of PEI (2) PEI networking (3) PEI carboxylation	10 ppm BSA@5.5 MPa 30 ppm sodium alginate@5.5 MPa	31.5 32.9	15.4 9.1	95.4 98.4	Non applicable		43

15958 | *J. Mater. Chem. A*, 2016, **4**, 15945–15960

This journal is © The Royal Society of Chemistry 2016

the shaking time was prolonged to 24 h. We can see that the bacteria experienced rapid reproduction during the 24 h shake period. In contrast with the former results, the agar plates corresponding to the PA-*g*-PEG/TAEA membrane were also filled with colonies, while for the PA-*g*-PEG/SMZ membrane, few colonies could still be seen.

By counting the bacteria colonies, the bacterial concentration and bacterial inhibition rate results were analyzed and are shown in Fig. 16. The initial bacteria suspension concentration was 4.0×10^5 CFU mL^{-1}; *S. aureus* seemed to achieve a relatively fast reproduction rate due to the high activity. The bacterial inhibition rate of the PA-*g*-PEG/TAEA membrane was around 70.0% for the two types of bacteria for 4 h cultures, while the value for the PA-*g*-PEG/SMZ membrane was above 90.0%. The results were obviously different after shaking for 24 h. The PA-*g*-PEG/TAEA membrane did not show sufficient antibacterial properties, and the bacterial inhibition rate dropped dramatically to below 30%, indicating that the inhibition of bacteria by the TAEA molecules cannot compete with the high reproductive rate of the bacteria. However, the value of the PA-*g*-PEG/SMZ membrane still remained above 95.0%, showing superior and stable inhibition effects. The different results for the two modified membranes are likely due to the different antibacterial mechanisms of TAEA and SMZ. For TAEA, the mechanism is similar to that of chitosan, which is associated with the presence of free NH$_2$ groups.[54] TAEA provides the membrane with a polycationic surface after modification, which is advantageous for bacterial adhesion through electrostatic attraction. The bound bacteria gradually becomes deformable due to uneven distribution of the negative charge on the cytoplasm and cell membrane, followed by physical fracture and the flowing out of moisture, proteins and other substances. Eventually, the bacteria die from pressure and lack of nutrition. Generally, TAEA requires a relatively long time and several steps to take effect. In contrast to TAEA, SMZ takes effect *via* a more rapid antibacterial process. From a bacteriological point of view, tetrahydrofolic acid participates in the synthesis of nucleic acids that essentially work as building blocks of DNA and RNA of bacteria, while SMZ acts as a competitive inhibitor of the enzyme dihydropteroate synthease, which catalyses the conversion of *para*-aminobenzoate to dihydropteroate, a key step in bacterial reproduction.[55,56] Therefore, SMZ is able to kill bacteria by preventing bacterial reproduction in its critical step, which is a more straightforward method. This is the main reason that SMZ shows obviously higher and more stable antibacterial activity than TAEA.

11. Comparison with other antifouling and antibacterial TFC membranes

The surface modification of RO membranes to address fouling problems has attracted great attention for a long time. Herein, we summarize some representative examples in Table 2. It should be noted that quantitative comparison of the antifouling or antibacterial properties of the membranes is difficult, as each membrane was subjected to exclusive test conditions. However, the ease and effectiveness of the modification method in this work are clearly demonstrated. A one-step process was used to impart both antifouling and antibacterial properties to the membrane. Both the FRR values and the antibacterial efficiency values of the obtained membranes are at the high end of the listed values. As a comparison, most other reports investigated only one type of fouling test, and multi-step modification processes were used. Note that "Non applicable" means that the related investigation was not conducted.

Conclusions

In this work, a novel surface modification strategy based on the Ugi four-component reaction (Ugi-4CR) was used to prepare antifouling and antibacterial RO membranes. Two modifying agents were simultaneously grafted in a "one-pot" procedure under mild conditions; this procedure is simple to conduct and demonstrates high efficiency. The obtained PA-*g*-PEG/SMZ membrane not only shows excellent resistance to BSA adsorption and inorganic salt deposition, but also shows superior antibacterial activity, which is demonstrated by a 98.6% bacterial inhibition rate even for a 24 h culture. With the additional benefits of commercially available modification agents, a simple method, and mild conditions, this grafting chemistry based on a multicomponent reaction not only provides a simple way to prepare antifouling and antibacterial RO membranes but also has great potential in the development of more applications of multifunctional modification on membrane surfaces.

Acknowledgements

References

1 X. Garcia and D. Pargament, *Resour., Conserv. Recycl.*, 2015, **101**, 154–166.

2 D. Li and H. Wang, *J. Mater. Chem.*, 2010, **20**, 4551–4566.

3 N. Misdan, W. J. Lau and A. F. Ismail, *Desalination*, 2012, **287**, 228–237.

4 J. E. Cadotte, R. J. Petersen, R. E. Larson and E. E. Erickson, *Desalination*, 1980, **32**, 25–31.

5 G. D. Kang and Y. M. Cao, *Water Res.*, 2012, **46**, 584–600.

6 W. Guo, H. H. Ngo and J. Li, *Bioresour. Technol.*, 2012, **122**, 27–34.

7 N. H. Lin, M.-m. Kim, G. T. Lewis and Y. Cohen, *J. Mater. Chem.*, 2010, **20**, 4642–4652.

8 L. Chen, H. Thérien-Aubin, M. C. Wong, E. M. Hoek and C. K. Ober, *J. Mater. Chem. B*, 2013, **1**, 5651–5658.

9 R. A. Al-Juboori and T. Yusaf, *Desalination*, 2012, **302**, 1–23.

10 J. Mansouri, S. Harrisson and V. Chen, *J. Mater. Chem.*, 2010, **20**, 4567–4586.

11 S. B. Singh, *Bioorg. Med. Chem. Lett.*, 2014, **24**, 3683–3689.

12 M. S. Rahaman, H. Thérien-Aubin, M. Ben-Sasson, C. K. Ober, M. Nielsen and M. Elimelech, *J. Mater. Chem. B*, 2014, **2**, 1724–1732.

13 X. Zhao and C. He, *ACS Appl. Mater. Interfaces*, 2015, **7**, 17947–17953.

14 H. J. Kim, D.-G. Kim, H. Yoon, Y.-S. Choi, J. Yoon and J.-C. Lee, *Adv. Mater. Interfaces*, 2015, **2**, 1500298.

15 Y. Li, Y. Su, X. Zhao, X. He, R. Zhang, J. Zhao, X. Fan and Z. Jiang, *ACS Appl. Mater. Interfaces*, 2014, **6**, 5548–5557.

16 L. Zou, I. Vidalis, D. Steele, A. Michelmore, S. P. Low and J. Q. J. C. Verberk, *Fuel Abstr. Curr. Titles*, 2011, **369**, 420–428.

17 A. Tiraferri, C. D. Vecitis and M. Elimelech, *ACS Appl. Mater. Interfaces*, 2011, **3**, 2869–2877.

18 Y. Xia, C. Cheng, R. Wang, C. Nie, J. Deng and C. Zhao, *J. Mater. Chem. B*, 2015, **3**, 9295–9304.

19 Y. Sui, X. Gao, Z. Wang and C. Gao, *J. Membr. Sci.*, 2012, **394**, 107–119.

20 I. Sawada, R. Fachrul, T. Ito, Y. Ohmukai, T. Maruyama and H. Matsuyama, *J. Membr. Sci.*, 2012, **387–388**, 1–6.

21 R. C. Cioc, E. Ruijter and R. V. Orru, *Green Chem.*, 2014, **16**, 2958–2975.

22 M. M. Khan, R. Yousuf and S. Khan, *RSC Adv.*, 2015, **5**, 57883–57905.

23 X.-X. Deng, L. Li, Z.-L. Li, A. Lv, F.-S. Du and Z.-C. Li, *ACS Macro Lett.*, 2012, **1**, 1300–1303.

24 O. Kreye, T. Tóth and M. A. Meier, *J. Am. Chem. Soc.*, 2011, **133**, 1790–1792.

25 I. Ugi, S. Lohberger and R. Karl, *Compr. Org. Synth.*, 1991, **2**, 1083–1109.

26 B. Yang, Y. Zhao, Y. Wei, C. Fu and L. Tao, *Polym. Chem.*, 2015, **6**, 8233–8239.

27 A. Sehlinger, P.-K. Dannecker, O. Kreye and M. A. R. Meier, *Macromolecules*, 2014, **47**, 2774–2783.

28 B. Yang, Y. Zhao, C. Fu, C. Zhu, Y. Zhang, S. Wang, Y. Wei and L. Tao, *Polym. Chem.*, 2014, **5**, 2704–2708.

29 A. Sehlinger, K. Ochsenreither, N. Bartnick and M. A. R. Meier, *Eur. Polym. J.*, 2015, **65**, 313–324.

30 B. Yang, Y. Zhao, S. Wang, Y. Zhang, C. Fu, Y. Wei and L. Tao, *Macromolecules*, 2014, **47**, 5607–5612.

31 B. Yang, Y. Zhao, X. Ren, X. Zhang, C. Fu, Y. Zhang, Y. Wei and L. Tao, *Polym. Chem.*, 2014, **6**, 33–40.

32 M. Mondal and S. De, *RSC Adv.*, 2015, **5**, 38948–38963.

33 C. Jimmy and H. YukáTang, *J. Mater. Chem.*, 2002, **12**, 81–85.

34 K. El-Refaie, S. D. Worley and B. Roy, *Biomacromolecules*, 2007, **8**, 1359–1384.

35 M. He, H. Xiao, Y. Zhou and P. Lu, *J. Mater. Chem. B*, 2015, **3**, 3704–3713.

36 M. Ginic-Markovic, T. G. Barclay, K. T. Constantopoulos, E. Markovic, S. R. Clarke and J. G. Matisons, *Desalination*, 2015, **369**, 37–45.

37 M. Elimelech, W. H. Chen and J. J. Waypa, *Desalination*, 1994, **95**, 269–286.

38 L. Ni, J. Meng, X. Li and Y. Zhang, *J. Membr. Sci.*, 2014, **451**, 205–215.

39 S. Kim and E. M. V. Hoek, *Desalination*, 2007, **202**, 333–342.

40 W. Chen, Y. Su, J. Peng, Y. Dong, X. Zhao and Z. Jiang, *Adv. Funct. Mater.*, 2011, **21**, 191–198.

41 W. Hu, S. Chen, X. Li, S. Shi, W. Shen, X. Zhang and H. Wang, *Mater. Sci. Eng., C*, 2009, **29**, 1216–1219.

42 H. J. Kim, Y. Baek, K. Choi, D.-G. Kim, H. Kang, Y.-S. Choi, J. Yoon and J.-C. Lee, *RSC Adv.*, 2014, **4**, 32802–32810.

43 H. Choi, Y. Jung, S. Han, T. Tak and Y.-N. Kwon, *J. Membr. Sci.*, 2015, **486**, 97–105.

44 S. Xia, L. Yao, Y. Zhao, N. Li and Y. Zheng, *Chem. Eng. J.*, 2015, **280**, 720–727.

45 M. Hashino, T. Katagiri, N. Kubota, Y. Ohmukai, T. Maruyama and H. Matsuyama, *J. Membr. Sci.*, 2011, **366**, 389–397.

46 I. H. Huisman, P. Prádanos and A. Hernández, *J. Membr. Sci.*, 2000, **179**, 79–90.

47 S. Lee and M. Elimelech, *Environ. Sci. Technol.*, 2006, **40**, 980–987.

48 G. B. Sigal, M. Mrksich and G. M. Whitesides, *J. Am. Chem. Soc.*, 1998, **120**, 3464–3473.

49 X. Fan, Y. Su, X. Zhao, Y. Li, R. Zhang, T. Ma, Y. Liu and Z. Jiang, *J. Membr. Sci.*, 2015, 499.

50 B. P. Tripathi, N. C. Dubey and M. Stamm, *J. Membr. Sci.*, 2014, **453**, 263–274.

51 L. Song and M. Elimelech, *J. Chem. Soc., Faraday Trans.*, 1995, **91**, 3389–3398.

52 M. Chaussemier, E. Pourmohtasham, D. Gelus, N. Pécoul, H. Perrot, J. Lédion, H. Cheap-Charpentier and O. Horner, *Desalination*, 2015, **356**, 47–55.

53 D. Liu, F. Hui, J. Ledion and F. Li, *Environ. Technol.*, 2011, **32**, 1017–1030.

54 S. C. M. Fernandes, P. Sadocco, A. Alonso-Varona, T. Palomares, A. Eceiza, A. J. D. Silvestre, I. Mondragon and C. S. R. Freire, *ACS Appl. Mater. Interfaces*, 2013, **5**, 3290–3297.

55 W. Baran, E. Adamek, J. Ziemianska and A. Sobczak, *J. Hazard. Mater.*, 2011, **196**, 1–15.

56 S. Mondal, S. M. Mandal, T. K. Mondal and C. Sinha, *Spectrochim. Acta, Part A*, 2015, **150**, 268–279.

57 A. Bera, R. M. Gol, S. Chatterjee and S. K. Jewrajka, *Desalination*, 2015, **360**, 108–117.

58 J. Wu, Z. Wang, W. Yan, Y. Wang, J. Wang and S. Wang, *J. Membr. Sci.*, 2015, **496**, 58–69.

15960 | *J. Mater. Chem. A*, 2016, **4**, 15945–15960

This journal is © The Royal Society of Chemistry 2016